ADD

Interaction Notes
Note 426
November 1981

Transient Response of the E-4B Trailing-Wire Antenna

by
F.C. Yang
V. Tatoian
L. Marin

The Dikewood Corp.
Santa Monica, California

Abstract

The transient response of the trailing-wire antenna on the E-4B is calculated. It is found that the largest peak value of the induced current occurs when the incident electromagnetic field strikes the antenna near grazing from behind. The critical angles and the associated time-domain waveforms are calculated for both the short and long wires. An equivalent circuit for the antenna current at the point where each wire enters the aircraft is constructed. The impedance and open-circuit voltage properties of the circuit are investigated. This equivalent circuit is used to define requirements for a pulse generator that simulates the early portion of the antenna wire current.

ACKNOWLEDGEMENT

We wish to thank Drs. M. Harrison, J.P. Castillo, and C.E. Baum of the Air Force Weapons Laboratory for many helpful discussions. Many technical discussions and much help was given to us during the course of this work by our collegue Dr. K.S.H. Lee.

CONTENTS

ILLUSTRATIONS

TABLE

SECTION I

INTRODUCTION

To fully assess the electromagentic pulse (EMP) hardness of the E-4B requires that one include all possible mission configurations of the system. One configuration that potentially can have a large impact upon the final hardness assessment of the aircraft is the one with the VLF/LF trailing-wire antenna (TWA) extended. The extreme lengths of the wires (many kilometers long) make it impossible to illuminate them with a simulated EMP of any substantial magnitude. On the other hand, the presence of the trailing-wire antenna will substantially alter the EMP response of the E-4B. In particular, it is expected that the low frequency response of the system will be considerably enhanced by the presence of these wires. It is therefore a great need of being able to simulate the effects of the TWA on the EMP response of the E-4B. One way of doing that is to directly inject currents onto the aircraft at the points where the wires exit the aircraft. Different methods of doing that are presented in Reference 1. In order to define specifications for required pulsers it is necessary to have some knowledge about the EMP induced current on the antenna wires. These calculations can also be used in estimating the achievable simulation fidelity with any existing pulsers.

The transient EMP response of the TWA is analyzed in this report. It is assumed that the response falls within the linear regime, e.g. no corona effects are included in the model. Estimates of corona effects on the trailing-wire antenna response can be found in Reference 2. The quantities of particular interest are the time histories of the induced currents at the points where the antenna wires exit from the aircraft. It is assumed that both the aircraft and the antenna wires are illuminated by a pulsed electromagnetic wave. The direction of incidence and polarization of the electromagnetic pulse is shown in Figure 1. The waveform of the incident wave is taken to be a double exponential such that

$$\underline{E}(\underline{r},t) = E_0(\hat{z}\cos\theta - \hat{x}\sin\theta)\, g(t + x\cos\theta/c + z\sin\theta/c)$$

where E_0 is the strength of the incident field and

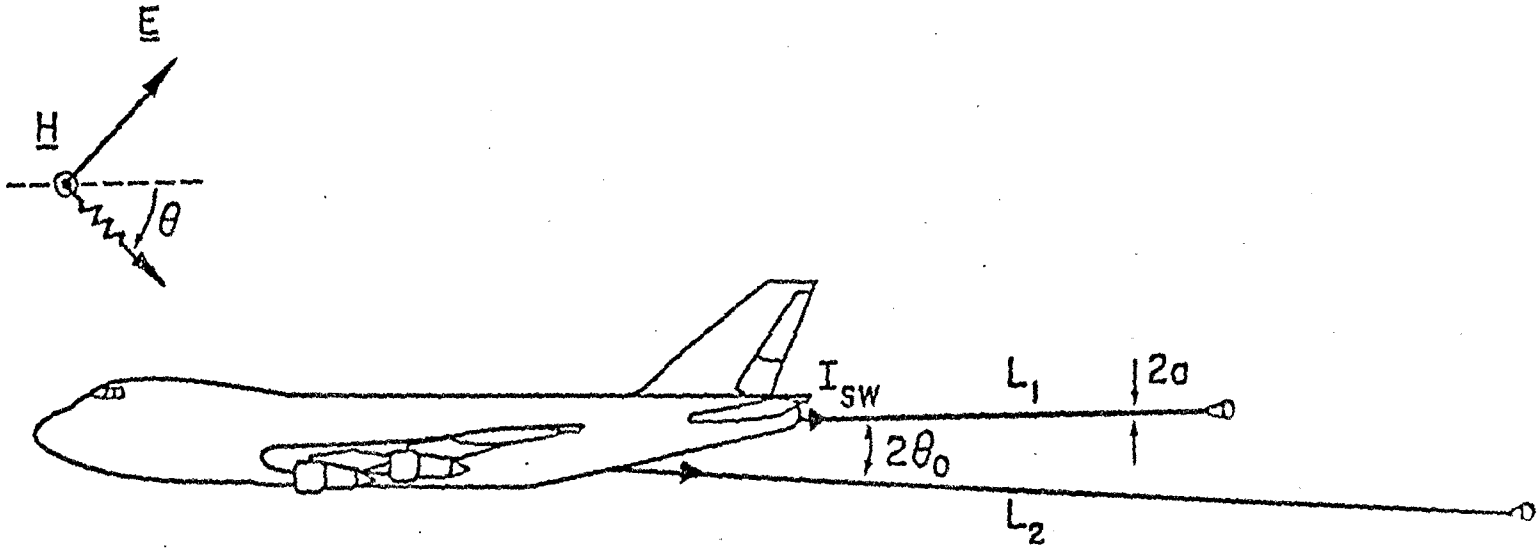

$L_1 = 1.2\,km$, $L_2 = 7.2\,km$, $a = 2mm$,

$\theta_0 = 3°$, $0° < \theta < 180°$, $\phi = \theta - 2\theta_0$

$$g(t) = \left[\exp(- t/\tau_f) - \exp(- t/\tau_r) \right] U(t)$$

Here, τ_r (= 2 ns) is the pulse rise time, τ_f (= 250 ns) is the pulse fall time and U(t) is the unit step function. The origin of the coordinate system is located at the tail of the aircraft(i.e. the exit point of the short antenna wire).

The starting point of the time-domain calculations is the frequency-domain response calculated in Reference 3. The results in this reference can be expanded to reveal the traveling-wave nature of the current on each wire. In fact, the wire current can be viewed as a sequence of repeatedly reflected pulses, the initial pulse being generated by the incident EMP. The time-domain results are obtained by taking an inverse Fourier transform of the expanded frequency-domain expressions.

The required mathematical machinery is discussed in Section II with some of the details relegated to Appendices A and B. The results of the performed calculations are presented in Section III. An equivalent circuit for the wire current is derived in Section IV based on the transient response calculations. This circuit is used in Section V to investigate requirements for pulsers simulating the transient response of the antenna wire.

SECTION II

FORMULATION

Time-domain expressions for the induced wire currents are reduced in this section. In principle, the time-domain results could be obtained by performing a numerical inverse Fourier transform of the frequency - domain results in Reference 3. The rapid variation of the response prohibits however this approach. Rather, some expansions and simplifications need to be done to obtain an expression which is tractable for inverse transformation.

It was observed in References 3 and 4 that the loading presented by the short wire feed has a negligable influence on the induced wire current for most frequencies. This fact and the fact that the surge arrestors installed on the system are expected to be activated by the EMP induced currents and voltages on the wires makes us use a model where both wires are short circuited to the aircraft. Thus, using the notations of Reference 3 we calculate I^{SW}_{ind} and I^{LW}_{ind}. From the analyst's point of view, this has the net effect of somewhat simplifying the problem.

As mentioned in the introduction, one expects the induced wire current to exhibit a traveling wave nature due to successive reflections of the initial pulse at each wire end. This behavior can be seen mathematically by expanding the current response in a power series in $F(L_1)$ and $F(L_2)$ (the symbols are all defined in Reference 3). Each increase in power of these functions represent an additional reflection at a wire end. As time elapses the magnitude of the reflected pulses get smaller and smaller due to radiation losses and dispersion of the pulse. Thus, and investigation of the current pulse initially induced by the incident EMP plus the current due to one reflection should be sufficient to describe the general nature of the wire current. By studying the current in the time interval $0 \leq t \leq 2L_1/c$ one achieves this goal.

Some algebraic manipulations on the expressions derived in Reference 3 allows one to obtain the following frequency-domain expression, the inverse Fourier transform of which results in a correct time-domain representation of the wire currents for $0 \leq t < 2L_1/c$

$$I^{SW}_{ind} \simeq I'_{ind} + \frac{\psi Z_o}{4\pi} \bar{Y}_a \left[(1 - \cos\theta)\, I_s(0,\theta) - 2\, I_s(L_1,\theta)\, R_1(\theta)\, F(L_1) \right]$$

$$+\frac{\psi Z_o}{4\pi}\,\bar{Y}_T\left[(1-\cos\phi)\,I_s(0,\phi)-2\,I_s(L_2,\phi)R_2(\phi)F(L_2)\right]\exp(jk\ell_4\cos\theta) \tag{1}$$

$$I_{ind}^{LW} = I'_{ind} + \frac{\psi Z_o}{4\pi}\,\bar{Y}_T\left[(1-\cos\theta)\,I_s(0,\theta)-2\,I_s(L_1,\theta)\,R_1(\theta)\,F(L_1)\right]$$

$$+\frac{\psi Z_o}{4\pi}\,\bar{Y}_a^{LW}\left[(1-\cos\phi)\,I_s(0,\phi)-2\,I_s(L_2,\phi)\,R_2(\phi)F(L_2)\right]\exp(jk\bar{\ell}_4\cos\theta) \tag{2}$$

where $\psi = -2\,\ell n\,(\Gamma ka) - j\pi$, $\Gamma = 1.781\ldots$, $Z_o(\approx 377\Omega)$ is the free space waveimpedance. The expressions for I'_{ind}, I''_{ind}, $\bar{Y}_a$, $\bar{Y}_T$, $\bar{Y}_a^{LW}$, $I_s(\xi,\theta)$, $R_1(\theta)$, $R_2(\theta)$, $F(\xi)$ are rather complicated and they can be found in Appendix A.

The various terms in Equations 1 and 2 have the following physical explanations

- I'_{ind} is the current on the short wire due to excitation of the aircraft alone
- I''_{ind} is the current on the long wire due to excitation of the aircraft alone
- the term multiplied by $\bar{Y}_a$ is the current on the short wire due to excitation of it alone
- the term multiplied by $\bar{Y}_a^{LW}$ is the current on the long wire due to excitation of it alone
- the terms multiplied by $\bar{Y}_T$ describe the respective wire current due to mutual coupling between the wires by way of the aircraft.

It was found in Reference 3 that the mutual coupling between the wires is very weak indeed. This means that the term including $\bar{Y}_T$ can be neglected in Equations 1 and 2. Futhermore, the quantity ψ varies logarithmically with the frequency. This is a very slow variation with frequency compared with the other quantities. To considerably simplify the calculations (and avoid a branch cut in the inverse Fourier integral) ψ will be given a constant value throughout the entire frequency regime. With these two additional observations one can proceed to evaluate the inverse Fourier integrals using residue calculus methods and obtain the following representations of the induced wire currents when the incident field is a double exponential field

$$I_{ind}^{SW}(t) = I_{SW}^{w}(t) + I_{SW}^{a}(t) \tag{3}$$

where

$$I^{w}_{SW}(t) \simeq \frac{4\pi c E_o}{Z_o \sin\theta[\psi - 2\ell n(0.5\sin\theta)]} \times$$

$$\times \left\{ 0.5(\tau_f - \tau_r)\left[(1-\cos\theta)\,U(t) - a_\theta U(t-t'_1)\right]\right.$$

$$+ \tau_r \left(\frac{Z_o\psi}{4\pi}\,\overline{Y}_a\right)_{k=\frac{j}{c\tau_r}} \left[(1-\cos\theta)\,V_r(t) - a_\theta\, V_r(t-t'_1)\right]$$

$$-\tau_f \left(\frac{Z_o\psi}{4\pi}\,\overline{Y}_a\right)_{k=\frac{j}{c\tau_f}} \left[(1-\cos\theta)\,V_f(t) - a_\theta\, V_f(t-t'_1)\right]$$

$$\left. + \mathrm{Re}\sum_{n=0}(2-\delta_{no})\frac{R_n}{k_n}\left(\frac{1}{jck_n+\tau_f^{-1}} - \frac{1}{jck_n+\tau_r^{-1}}\right)\left[(1-\cos\theta)\,V_n(t) - a_\theta V_n(t-t'_1)\right]\right\} \tag{4}$$

$$I^{a}_{SW}(t) \simeq \frac{4\pi c E_o}{\Omega Z_o}\left\{\frac{\tau_f-\tau_r}{2}\,N_1(0,t) - \tau_r \left.\frac{N_1(k,t)}{j\psi(\overline{T}_1 - \overline{T}_2\tan k\ell_5)/\Omega - \overline{T}_2}\right|_{k=j(c\tau_r)^{-1}}\right.$$

$$\left. + \tau_f \left.\frac{N_1(k,t)}{j\psi(\overline{T}_1 - \overline{T}_2\tan k\ell_5)/\Omega - \overline{T}_2}\right|_{k=j(c\tau_f)^{-1}}\right.$$

$$\left. - \mathrm{Re}\sum_{n=0}\frac{(2-\delta_{no})Q_n}{k_n}\left(\frac{1}{jck_n+\tau_f^{-1}} - \frac{1}{jck_n+\tau_r^{-1}}\right)N_1(k_n+j\beta_n,t)\right\} \tag{5}$$

and

$$I^{LW}_{ind}(t) = I^{w}_{LW}(t) + I^{a}_{LW}(t) \tag{6}$$

where

$$I^{w}_{LW}(t) \simeq \frac{4\pi c E_o}{Z_o \sin\theta\,[\psi - 2\,\ell n\,(0.5\sin\phi)]} \times$$

$$\times \left\{ 0.5(\tau_f - \tau_r)\left[(1-\cos\phi)\,U(t-t_2) - a_\phi\,U(t-t'_2)\right]\right.$$

$$\left. + \tau_r \left(\frac{Z_o\psi}{4\pi}\,\overline{Y}^{LW}_a\right)_{k=\frac{j}{c\tau_r}} \left[(1-\cos\phi)\,V_r(t-t_2) - a_\phi\, V_r(t-t'_2)\right]\right.$$

$$-\tau_f \left(\frac{Z_o \psi}{4\pi} \overline{Y}_a^{LW}\right)_{k=\frac{j}{c\tau_f}} \left[(1-\cos\phi)\, V_f(t-t_2) - a_\phi\, V_f(t-t_2')\right] \qquad (7)$$

$$+ \operatorname{Re} \sum_{n=o} (2-\delta_{no}) \frac{S_n}{k_n} \left(\frac{1}{jck_n + \tau_f^{-1}} - \frac{1}{jck_n + \tau_r^{-1}}\right) \left[(1-\cos\phi)\, V_n(t-t_2) - a_\phi V_n(t-t_2')\right] \Bigg\}$$

$$I_{LW}^a(t) \simeq \frac{4\pi c E_o}{\Omega Z_o} \Bigg\{ \frac{\tau_f - \tau_r}{2} N_2(0,t) - \tau_r \left. \frac{N_2(k,t)}{j\psi(\overline{T}_1 - \overline{T}_2 \tan k\ell_5)/\Omega - \overline{T}_2} \right|_{k=j(c\tau_r)^{-1}}$$

$$+ \tau_f \left. \frac{N_2(k,t)}{j\psi(\overline{T}_1 - \overline{T}_2 \tan k\ell_5)/\Omega - \overline{T}_2} \right|_{k=j(c\tau_f)^{-1}}$$

$$- \operatorname{Re} \sum_{n=o} (2-\delta_{no}) \frac{Q_n}{k_n} \left(\frac{1}{jck_n + \tau_f^{-1}} - \frac{1}{jck_n + \tau_r^{-1}}\right) N_2(k_n + j\beta_n,\, t) \Bigg\}$$

$$- \frac{4\pi c E_o}{\Omega Z_o} \left\{ (\tau_f - \tau_r)\, N_3(0,t) - \tau_f\, N_3\left(\frac{j}{c\tau_f},\, t\right) + \tau_r\, N_3\left(\frac{j}{c\tau_r}, t\right) \right\} \qquad (8)$$

The symbols used in Equations 4 through 8 are all defined in Appendix B.

It is observed that the expressions for I_{ind}^{SW} and I_{ind}^{LW} are composed of two terms. The term with the superscript "a" is the current that results from excitation of the aircraft whereas the term with the superscript "w" is the current that results from excitation of the respective wire itself. Each one of these expressions contains terms resulting from

- the residue associated with the pole from the rise time of the incident pulse ($k = j/c\tau_r$)
- the residue associated with the pole from the fall time of the incident pulse ($k = j/c\tau_f$)
- the residues associated with the poles from $\overline{Y}_a$ ($k = \pm k_n + j\beta_n$). These poles are all located in the upper half of the complex k-plane. For $n \geq 1$ these poles correspond approximately to the external resonances of the aircraft. The slight variation from these resonances are due to the presence of the wires. The $n = o$ pole results from the presence of the wires. Mathematically its occurance can be attributed

to ψ being a constant. Thus, this pole accounts for the branch-cut contribution one gets when using the frequency varying representation for ψ.

The numerical values of k_n and β_n are presented in Table 1 for the 9 lowest resonances.

TABLE 1. POLES OF $\overline{Y}_a$

n	k_n	β_n
0	0	0.00378
1	0.03129	0.00502
2	0.05480	0.00012
3	0.08229	0.00238
4	0.10475	0.00291
5	0.14378	0.00375
6	0.16569	0.00209
7	0.20020	0.00204
8	0.20989	0.01127

SECTION III

NUMERICAL RESULTS FOR THE INDUCED WIRE CURRENTS

The expressions derived in Section II were used to obtain numerical results for the induced wire currents. These results are presented in Figures 2 through 7.

The current on the short wire due to excitation of this wire only is presented in Figure 2 whereas the total wire current due to excitation of both the wires and the aircraft is shown in Figure 3. By comparing these two curves one observes that the effect of the aircraft excitation is very small on the short wire current. The maximum time-domain peak value (18 kA) of the current occurs for $\theta = 155°$. The rise time of the pulses are on the order of 200 - 400 ns which can be attributed to the fact that the induced wire current is roughly proportional to the time integral of the incident field. The narrow pulse width of the current for near grazing incidence is due to the small time lapse between the current initially induced by the incident wave and the current reflected off the outboard end of the wire.

The current induced on the long wire is shown in Figures 4 through 7. The current on the wire due to excitation of the wire itself is shown in Figure 4. The total current due to excitation of the wires and the aircraft is shown in Figures 5 through 7. Again it is found from the curves that the effect of the aircraft excitation is small on the wire current. The maximum time-domain peak value of 42 kA occurs for $\theta = 177°$ as can be seen in Figure 7. The pulse width for the worst case excitation is about the same ($\simeq 0.2\mu s$) for both wire currents. The angle $\theta = 195°$ is included to show the symmetry properties of the induced current. With the long wire drooping 6° from the horizon, the long-wire current has the following symmetry properties

$$I_{ind}^{LW}(t,\theta - 186°) = -I_{ind}^{LW}(t,186° - \theta)$$

The aircraft resonances have a somewhat stronger influence on the long-wire current than they do on the short-wire current.

It is observed that the peak value of the induced current on the wires is on the order of 2 kA to 10 kA for most angles of incidence. Only for near grazing angles of incidence does one get a current of peak amplitude substantially above this level. The width of the current pulse is much larger for the non-critical angles of incidence. It is also observed from the curves that the pulse width of the long-wire current is much larger than that of the short-wire current.

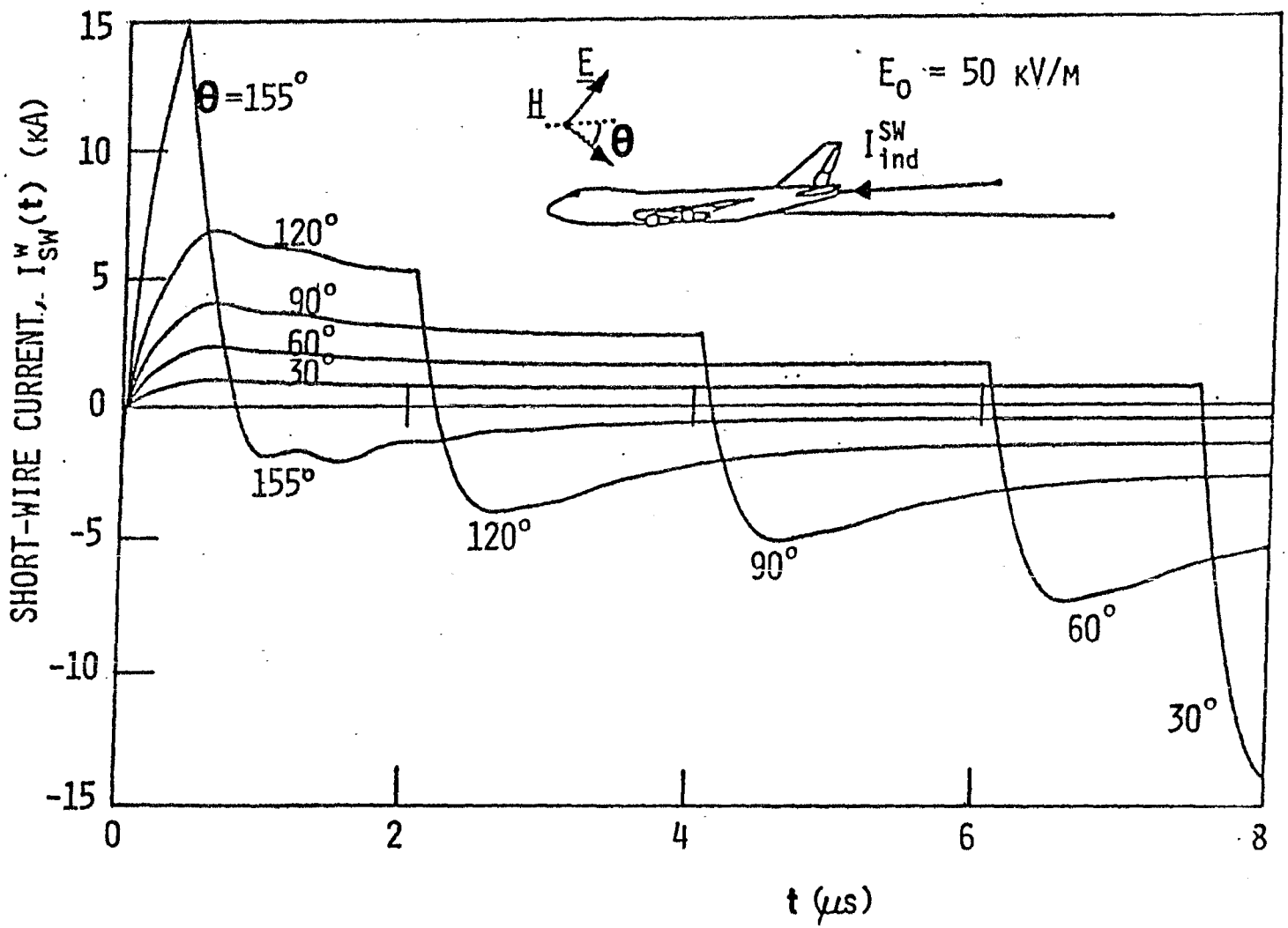

Figure 2. Time history of short-wire current due to excitation of the short-wire only.

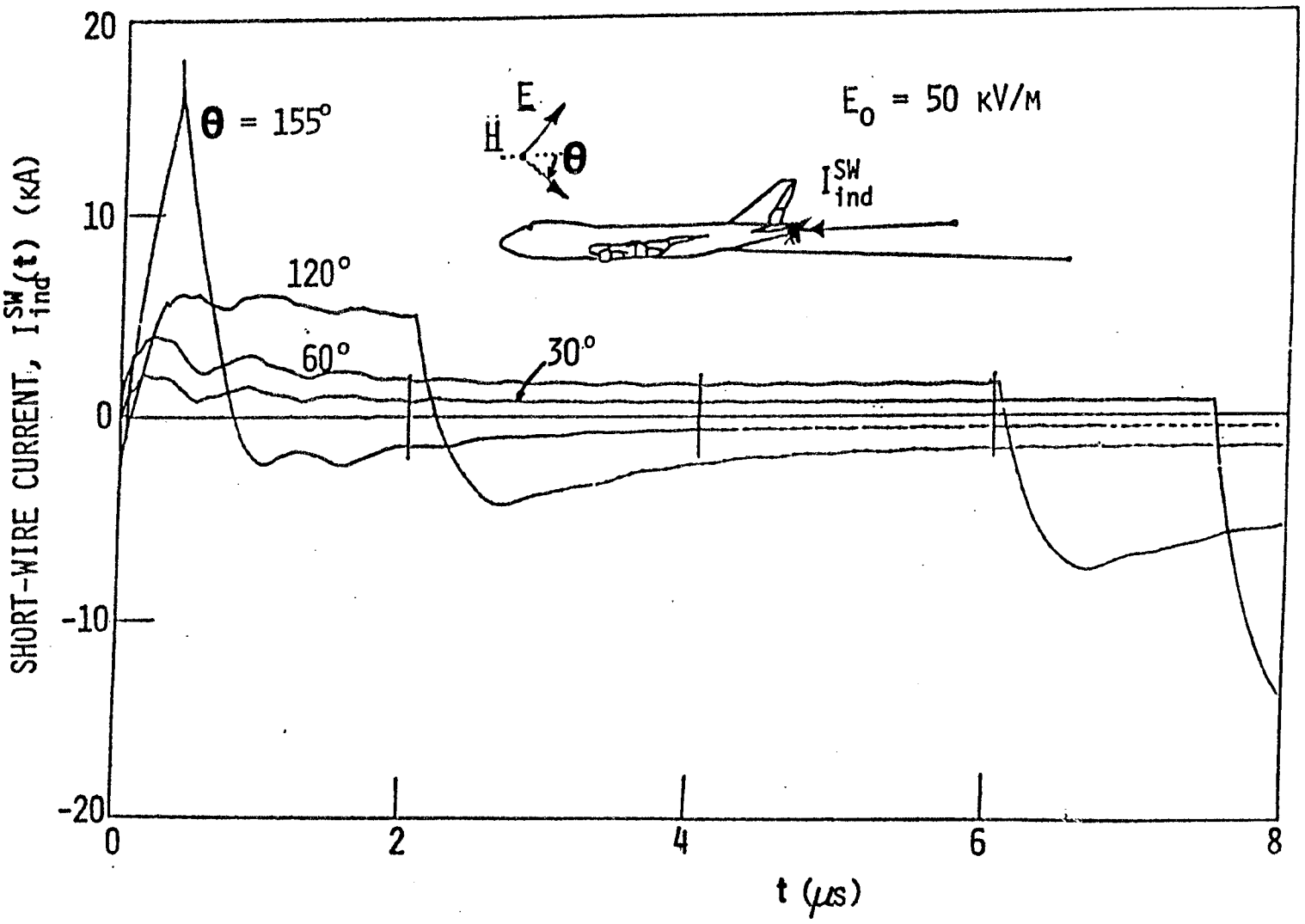

Figure 3. Time history of short-wire current due to excitation of the entire system (aircraft and wires).

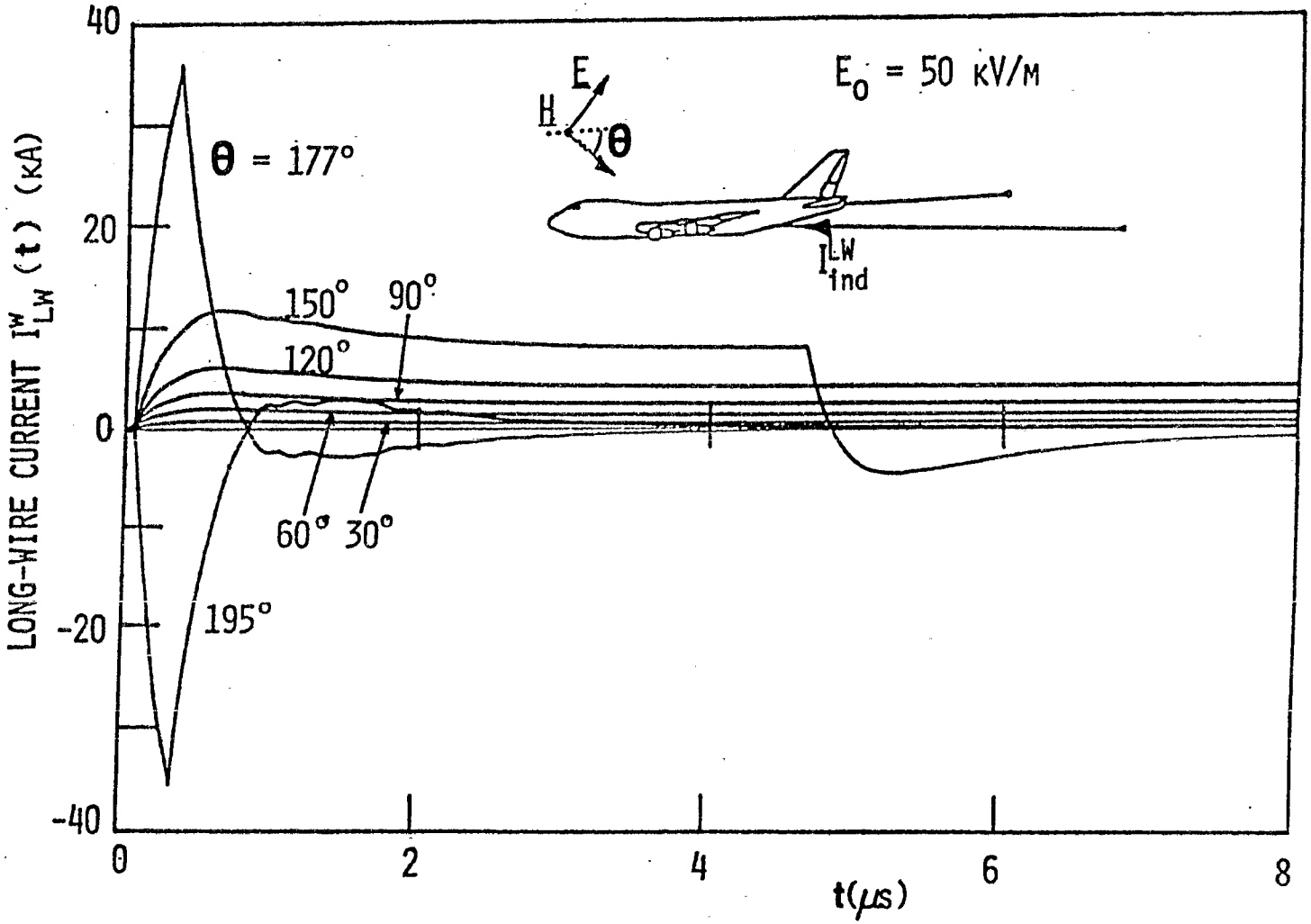

Figure 4. Time history of long-wire current due to excitation of the long wire only.

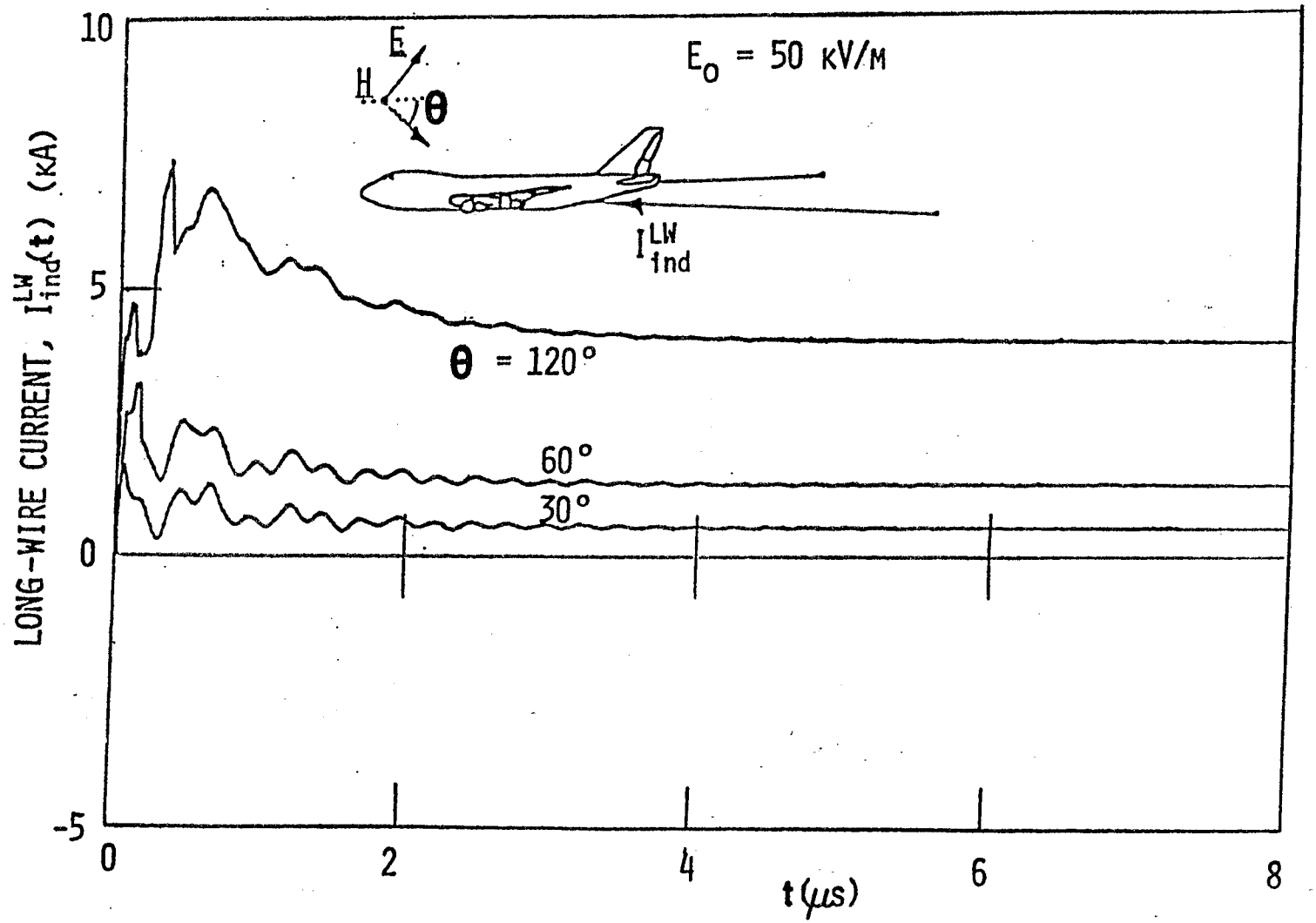

Figure 5. Time history of long-wire current due to excitation of the entire system (aircraft and wires) for θ = 30°, 60°, and 120°.

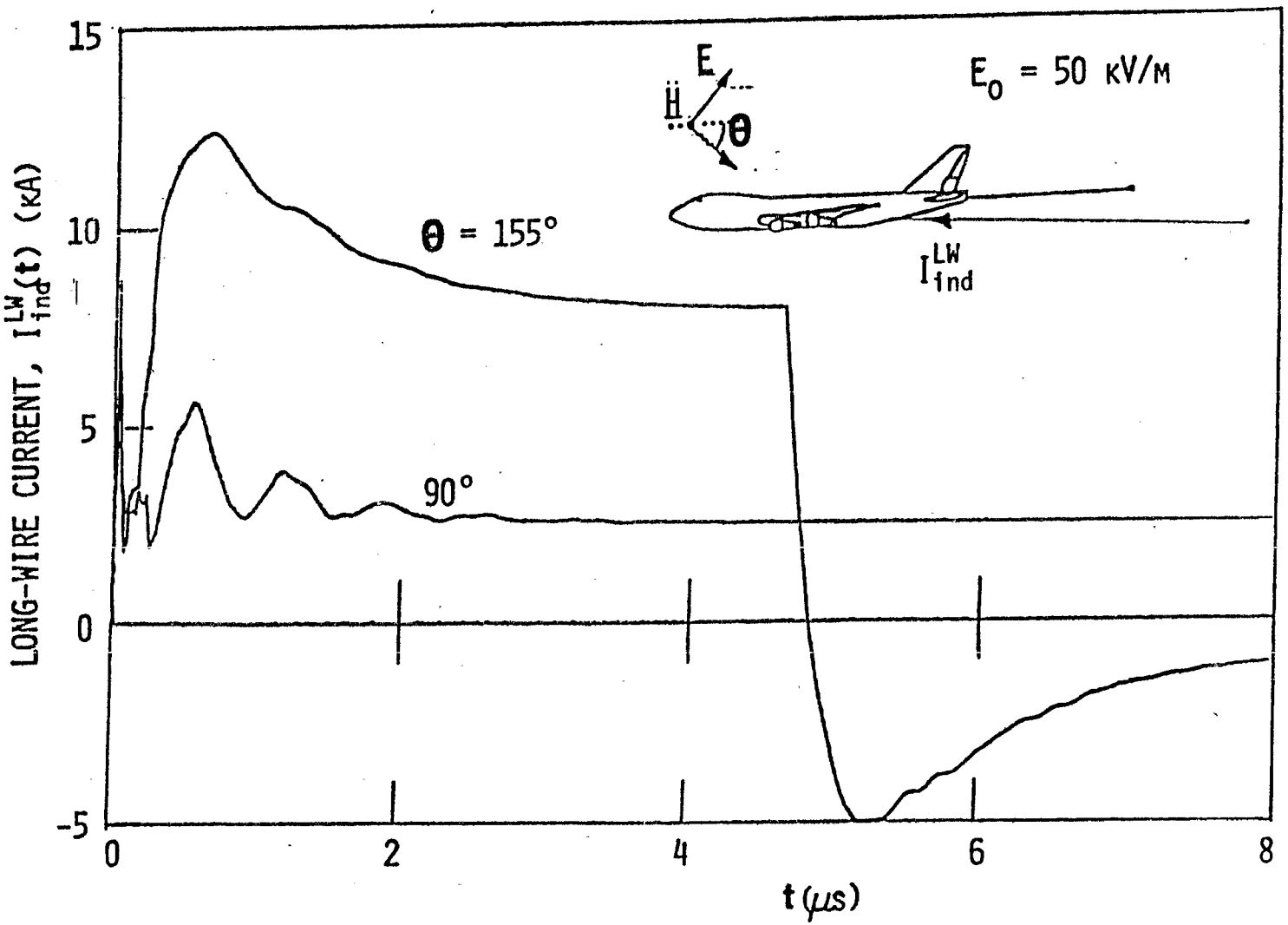

Figure 6. Time history of long-wire current due to excitation of the entire system (aircraft and wires) for θ = 90°and 155°.

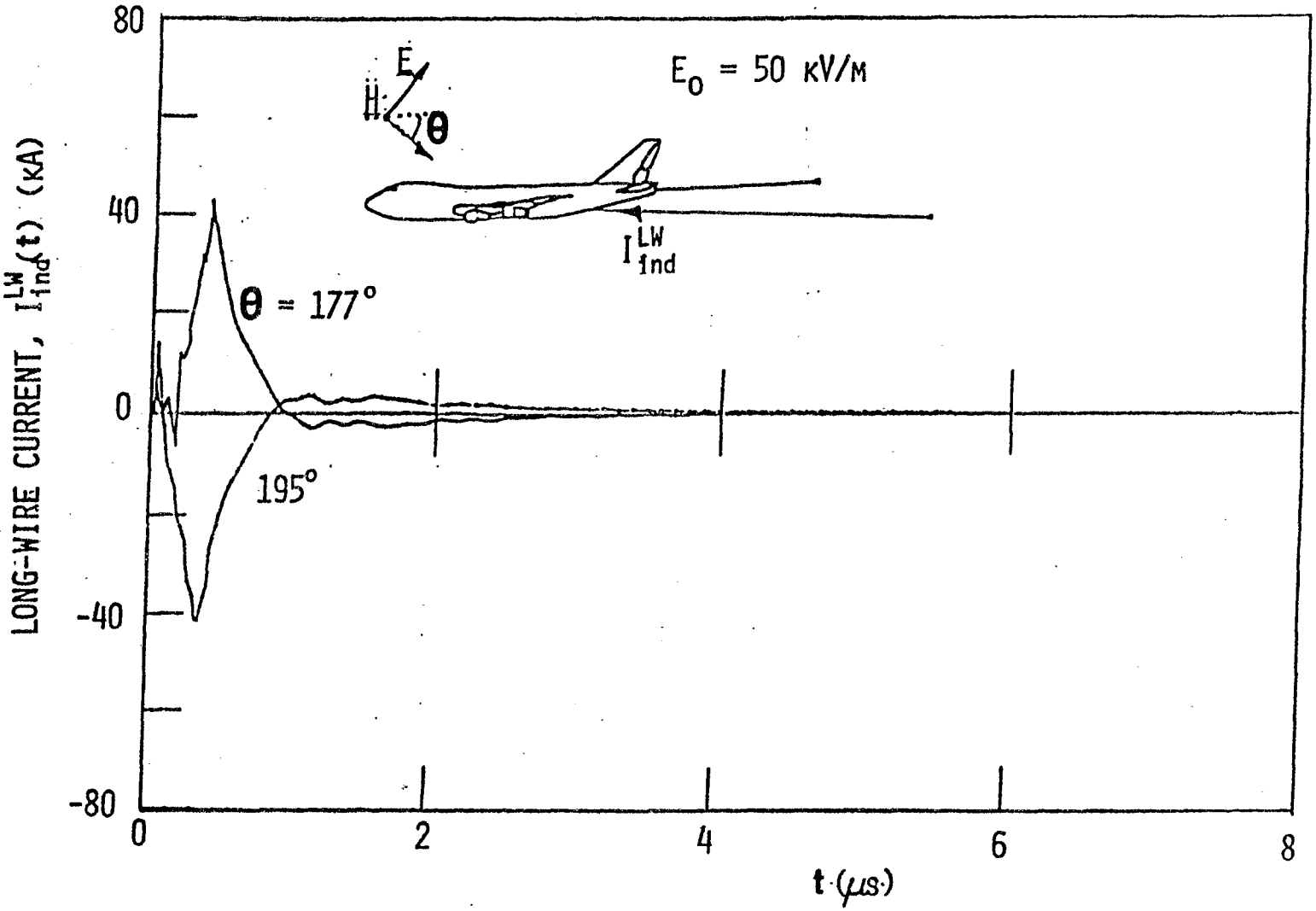

Figure 7. Time history of long-wire current due to excitation of the entire system (aircraft and wires) for θ = 177°and 195°.

SECTION IV

EQUIVALENT CIRCUIT FOR ANTENNA WIRE CURRENT

As mentioned in the introduction, one of the reasons for calculating the wire current is to determine requirements for direct-drive simulators. The results obtained so far in this report will be used in this section to derive an equivalent-circuit representation for the induced wire current. This equivalent circuit should be such that it results in the same induced current on the respective wire as the free field EMP excitation does.

Figure 8 shows the Thévenin equivalent circuit representation for the antenna wires from the point of view of the current injected onto the aircraft by the wires. The impedances Z_1 and Z_2 are the wire impedances and the voltages $V_1(t)$ and $V_2(t)$ are the open-circuit voltages induced by the EMP.

A. FREQUENCY-DOMAIN REPRESENTATION OF EQUIVALENT CIRCUIT

To derive an expression for the equivalent circuit we will use expressions for the frequency variation of the induced wire currents. These expressions have been derived in Reference 3 and they take the form of Equations 1 and 2 which are reproduced below.

$$I_{ind}^{SW} \simeq I'_{ind} + \frac{\psi Z_o}{4\pi} \bar{Y}_a \left[(1-\cos\theta)\, I_s(0,\theta) - 2\, I_s(L_1,\theta)\, R_1(\theta)\, F(L_1)\right]$$

$$+ \frac{\psi Z_o}{4\pi} \bar{Y}_T \left[(1-\cos\phi)\, I_s(0,\phi) - 2\, I_s(L_2,\phi)\, R_2(\phi)\, F(L_2)\right] \exp(jk\ell_4 \cos\theta) \qquad (1)$$

$$I_{ind}^{LW} \simeq I''_{ind} + \frac{\psi Z_o}{4\pi} \bar{Y}_T \left[(1-\cos\theta)\, I_s(0,\theta) - 2\, I_s(L_1,\theta)\, R_1(\theta) F(L_1)\right]$$

$$+ \frac{\psi Z_o}{4\pi} \bar{Y}_a^{LW} \left[(1-\cos\phi)\, I_s(0,\phi) - 2\, I_s(L_2,\phi)\, R_2(\phi)\, F(L_2)\right] \exp(jk\ell_4 \cos\theta) \qquad (2)$$

The quantities used in Equations 1 and 2 have been defined in Reference 3.

The physical significance of the various terms in Equations 1 and 2 are discussed in Section II of this report. To simulate I'_{ind} and I''_{ind} one could place the aircraft in a free field simulator such as the TRESTLE with the impedance properties of the wires appropriately accounted for. It was

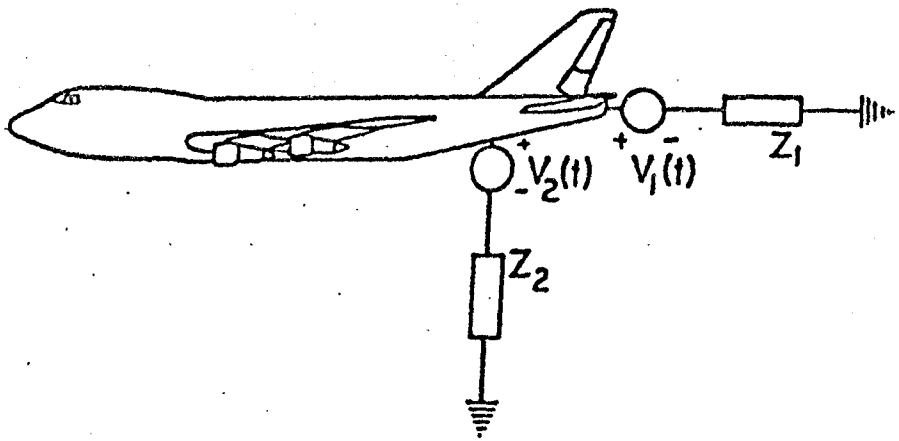

Figure 8. Thévenin equivalent circuit representation of the trailing-wire antenna.

however found in this report and in Reference 3 that the contributions from I'_{ind} and I''_{ind} on the respective wire current is very small. Similarly, it was found that the mutual coupling term (the term in Equations 1 and 2 containing the admittance $\bar{Y}_T$) is small. Thus, the important term to be considered in Equation 1 is the one containing $\bar{Y}_a$ and the important one in Equation 2 is the term containing $\bar{Y}_a^{LW}$.

The equivalent circuit derived in this report will be limited to the initial current pulse on the two wires. The expressions 1 and 2 show that the impedances of the wires are given by

$$Z_1 = Z_2 = Z_\infty = \psi Z_0/4\pi = -60\left[\ell n(\Gamma ka) + j\pi/2\right] \tag{10}$$

The open-circuit voltage on each wire is given by

$$V_1 = Z_\infty \left[(1 - \cos\theta)\, I_s(0,\theta) - 2\, I_s(L_1,\theta)\, R_1(\theta)\, F(L_1)\right] \tag{11}$$

$$V_2 = Z_\infty \left[(1 - \cos\phi)\, I_s(0,\phi) - 2\, I_s(L_2,\phi)\, R_2(\phi)\, F(L_2)\right] \exp(jk\ell_4 \cos\theta) \tag{12}$$

Expressions similar to these were derived in Reference 5, the main difference being that $R_1(\theta)$ and $R_2(\phi)$ were given the value of unity in Reference 5. As mentioned in Reference 3 that is a good approximation for these functions except near grazing angles of incidence.

B. TIME-DOMAIN REPRESENTATION OF EQUIVALENT CIRCUIT

The impedance and open-circuit voltage are synthesized separately. The frequency variation of Z_∞ is analyzed in Reference 5. It is seen there that the logarithmic frequency dependence makes the impedance variation stay within a factor of two over two decades of frequency variation. The average value of $Z_\infty = 660\Omega$ is chosen here.

To obtain time-domain expressions for the open circuit voltage we perform an inverse Fourier transform on Equations 1 and 2. With the wave-shape of the incident field being a double exponential function one obtains the following expressions for the two open-circuit voltages in Figure 8.

$$V_1(t) = \frac{\psi}{\psi - 2\ell n\,(0.5 \sin\theta)} \times$$

$$\times\left\{\frac{1-\cos\theta}{\sin\theta}\,V_o(t)-\frac{2}{\sin\theta}\left(1-\frac{1}{\psi_1'}\,\ell n\,\frac{t}{t-t_1'}\right)V_o(t-t_1')\right\} \tag{13}$$

$$V_2(t)=\frac{\psi}{\psi-2\,\ell n\,(0.5\sin\phi)}\times$$

$$\times\left\{\frac{1-\cos\phi}{\sin\phi}\,V_o(t-t_2)-\frac{2}{\sin\phi}\left(1-\frac{1}{\psi_2'}\,\ell n\,\frac{t-t_2}{t-t_2'}\right)V_o(t-t_2')\right\} \tag{14}$$

where $\psi \simeq 22$. With L_1 being 1200 m and L_2 being 7200 m, one has approximately $\psi_1' = 24$ and $\psi_2' = 26$. Futhermore,

$$t_1' = L_1(1+\cos\theta)/c, \tag{15}$$

$$t_2' = L_2(1+\cos\phi)/c + t_2, \quad t_2 = -\ell_4\cos\theta/c, \tag{16}$$

$$V_o(t) = c\,E_o\left[\tau_f\,(1-e^{-t/\tau_f}) - \tau_r(1-e^{-t/\tau_r})\right]U(t) \tag{17}$$

where τ_r, τ_f, E_o are respectively the rise-time, fall-time, electric field strength of the incident wave.

C. NUMERICAL RESULTS FOR OPEN CIRCUIT VOLTAGES

Equations 13 through 17 were used to obtain numerical values for $V_1(t)$ and $V_2(t)$. The results of these calculations are shown in Figure 9. In arriving at these results the values $\tau_r = 2$ns, $\tau_f = 250$ns, and $E_o = 50$k V/m were used. It is observed from these curves that the voltage slowly rises as the current wave is built up on the wire. The voltage begins to drop when the effects of the reflected signal from the outboard end of the antenna enters into the considered wire current. The time-domain peak values of the open circuit voltages for different angles of incidence are shown in Figure 10. It is seen from these curves how the peak values increase as the angle of incidence increases from nose-on incidence. A maximum peak value of 11 MV for the short wire occurs at $\theta = 155°$ whereas a maximum peak value of 26 MV occurs at $\theta = 177°$ for the long wire. These

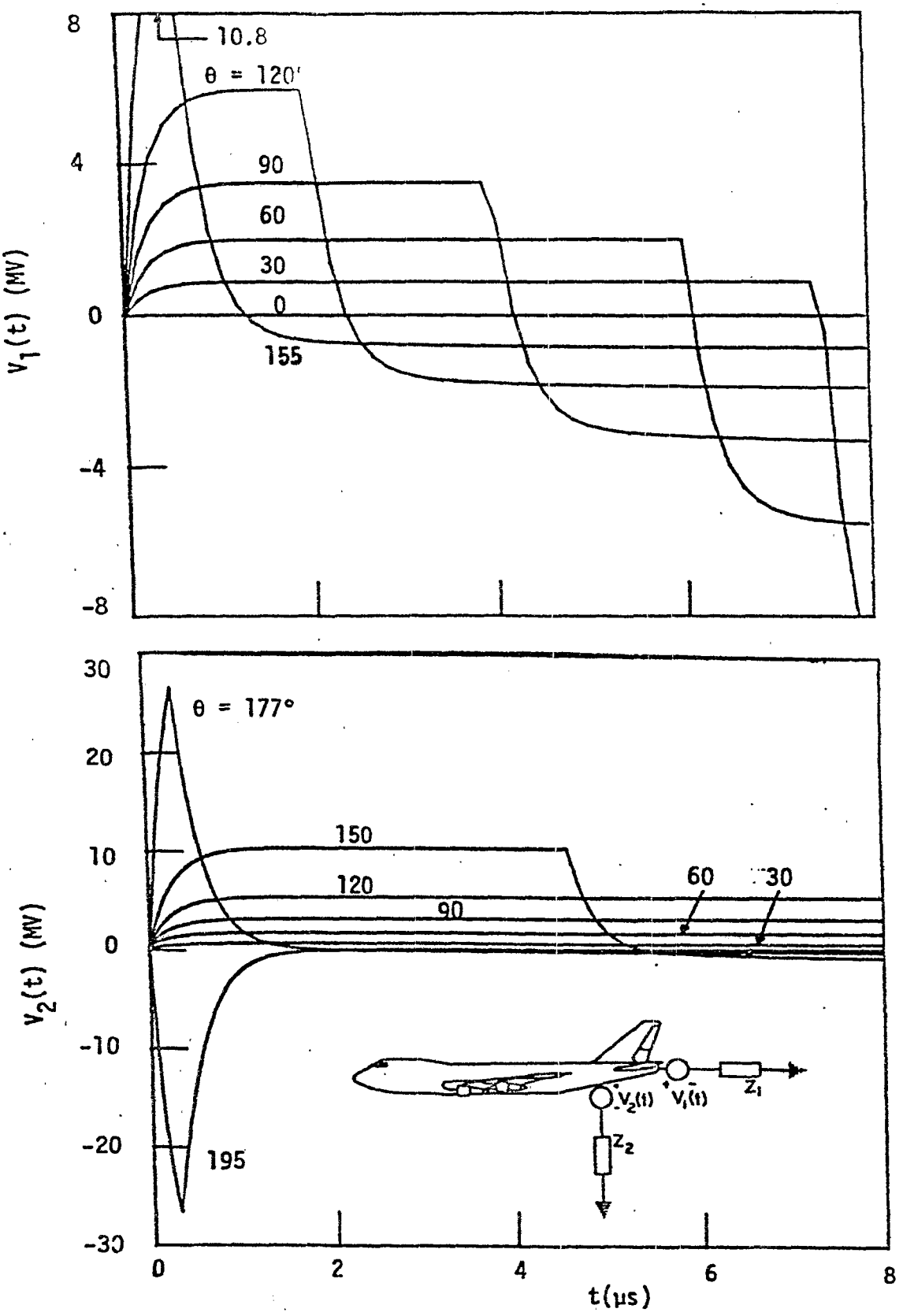

Figure 9. The open circuit voltages $V_1(t)$ and $V_2(t)$ of the equivalent circuit for the trailing-wire antenna.

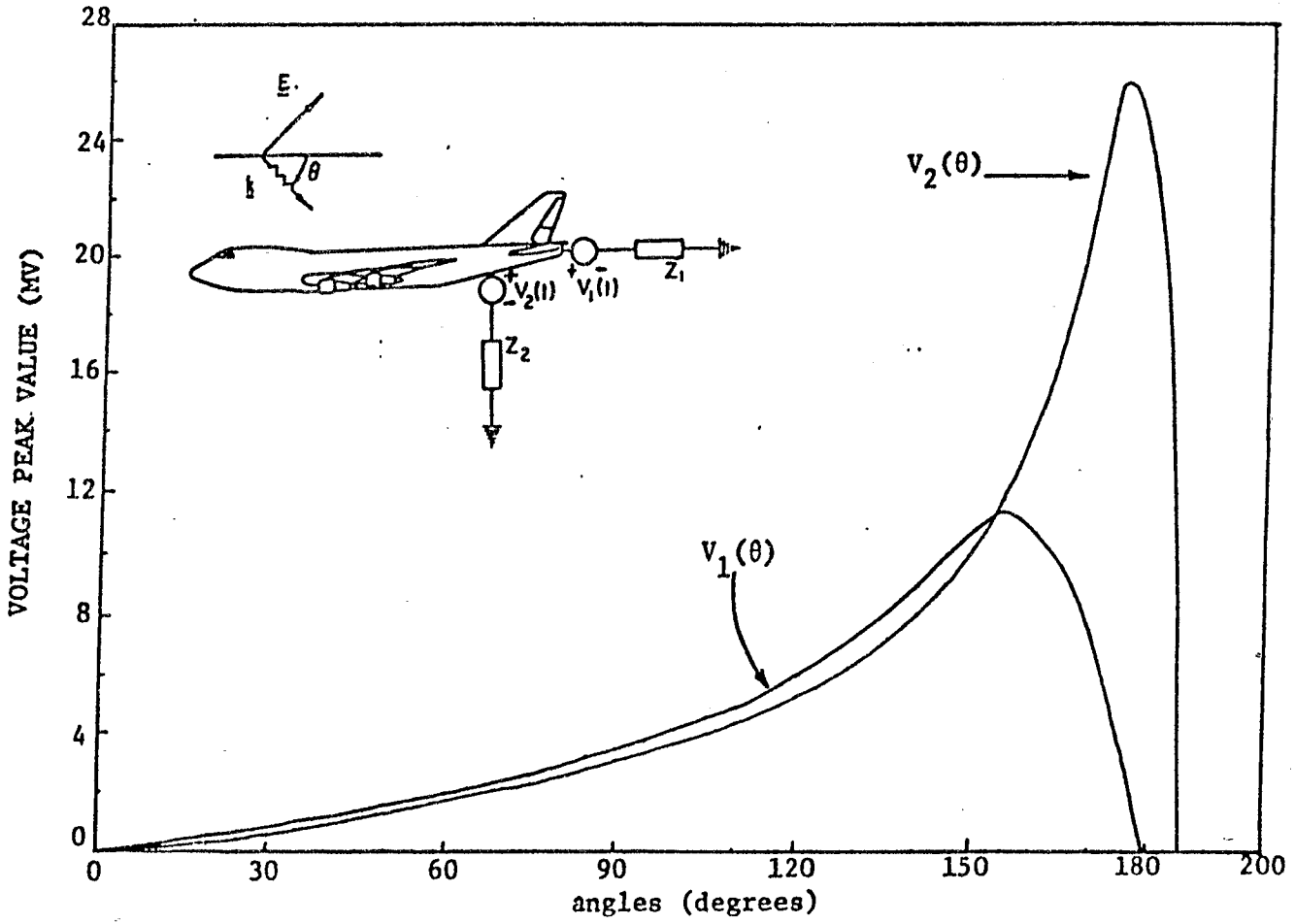

Figure 10. Peak values of the open circuit voltages $V_1(t)$ and $V_2(t)$ for different angles (θ) of the incident field.

angles are the same as those resulting in the largest peak value of the induced current. The fact that the voltage and current peak values occur for the same angles of incidence can be understood from the fact that it is the illumination of the respective wire alone that gives the largest contribution to the induced wire current.

Besides the time-domain peak value another important quantity characterizing the voltage pulse is its pulse width. One way of quantifying the pulse width is to observe the time of the first zero crossing (i.e. when the pulse first changes polarity). The variation of the first zero crossing of both the short-wire voltage and the long-wire voltage with the angle of incidence is shown in Figure 11.

To obtain network representations of $V_1(t)$ and $V_2(t)$ requires that one can synthesize $V_0(t)$ and $\ell n\ (1 + t'/t)\ V_0(t)$. Methods of synthesizing $V_0(t)$ are presented in Reference 5 and they will not be repeated here. To exactly realize $\ell n\ (1 + t'/t)\ V_0(t)$ is more difficult. However, the logarithmic term is a slowly varying function with time. Therefore it can be approximated by a constant with the value $\ell n\ (1 + t'/t_0)$ where $t_0 = 2L_1/c$ for the short wire and $t_0 = 2L_2/c$ for the long wire. With this approximation one can proceed to obtain equivalent circuits similar to those presented in Reference 5.

The main reason for not exploring the properties of the equivalent circuit in more detail stems from the large open-circuit voltages called for in them. To generate tens of megavolt voltages is beyond the state of the art. Rather, alternate methods must be devised where the current on each wire is simulated with a reasonable accuracy using state-of-the-art generators. In the next section we will investigate the feasibility of one such method.

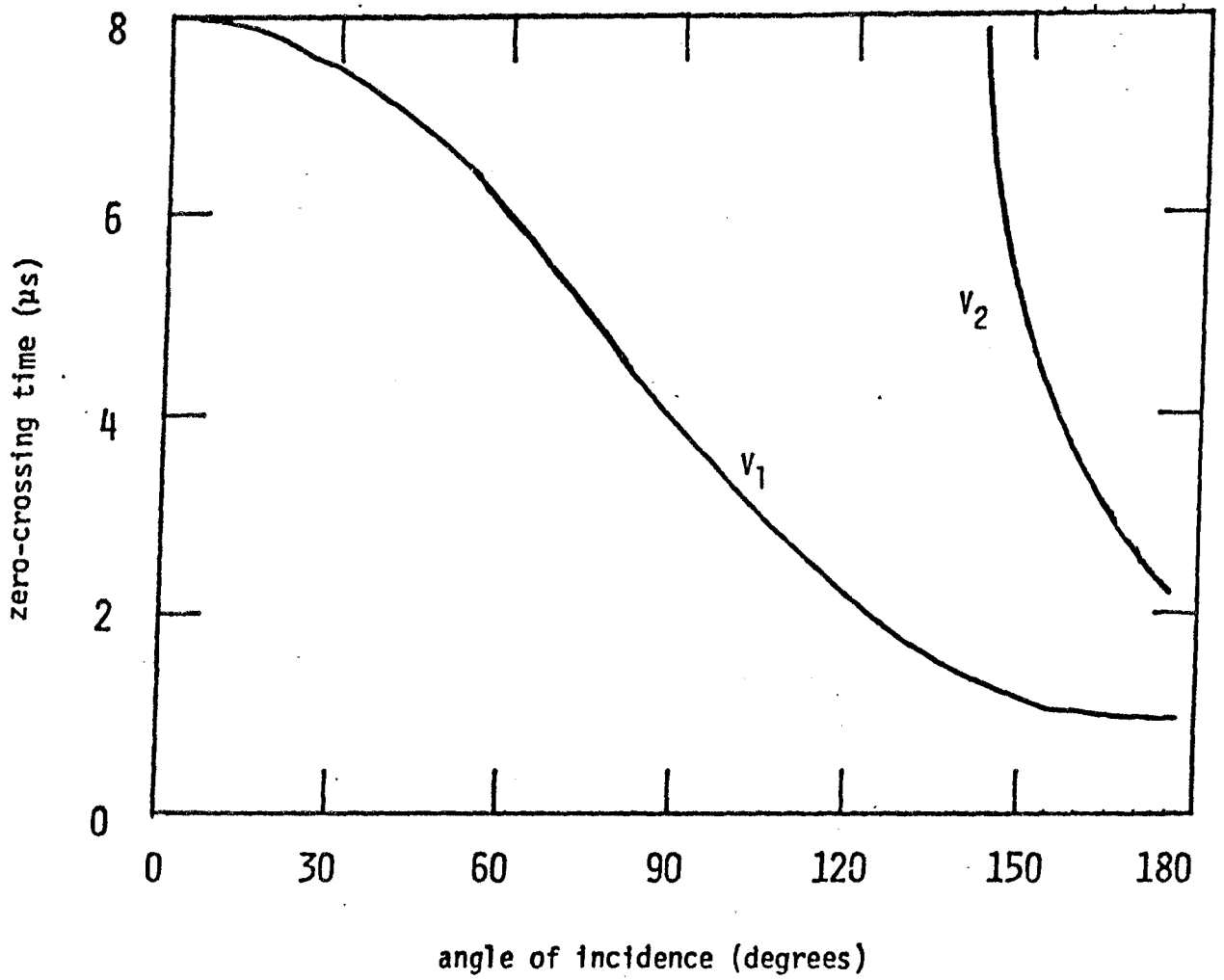

Figure 11. First zero crossing of $V_1(t)$ and $V_2(t)$ for different angles (θ) of the incident field.

SECTION V

FEASIBILITY OF SIMULATING ANTENNA WIRE CURRENT

The open-circuit voltage defined in the previous section reached values in the tens of magavolts. These large voltages are impractical to simulate with today's technology. Nevertheless, the equivalent circuit derived in the previous section can serve as the starting point for simulation methods of the short and long wire currents.

It was observed previously in this report that the current induced on the short and long wire are dominated by the excitation of the respective wire. The current on the short wire is given by $V_1 \bar{Y}_a$ whereas the current on the long wire is given by $V_2 \bar{Y}_a^{LW}$. Thus, if one can increase the antenna admittance $\bar{Y}_a$ (decrease the antenna impedance $\bar{Z}_a = 1/\bar{Y}_a$) by a factor n then one can decrease the voltage V_1 by the same factor n and yet the short wire current remains unchanged. The same argument applies equally well to the long-wire current. It is therefore of interest to investigate the properties of $\bar{Y}_a$ and $\bar{Y}_a^{LW}$.

The quantity $\bar{Y}_a$ is the admittance between the short wire and the aircraft as seen in Figure 12. This admittance depends both on the electrical properties of the aircraft and the antenna wire. It was found in the previous section that the magnitude of the wire impedance is on the order of 500 to 800 ohms. The aircraft capacitance is on the order of 2.5 nF which for a frequency of 1 MHz translates to an impedance of around 60 Ω. Thus, it is expected that the wire dominates the impedance for many frequencies. To quantify this fact more precisely we investigate the quantity $Z_\infty \bar{Y}_a$. If the quantity $\bar{Y}_a$ is dominated by the antenna wire then $Z_\infty \bar{Y}_a$ takes values close to unity. The futher $Z_\infty \bar{Y}_a$ deviates from unity the more important the presence of the aircraft becomes. A graph of $Z_\infty \bar{Y}_a$ ia shown in Figure 12. When reading the curve presented in this figure it should be kept in mind that $\bar{Y}_a$ denotes the antenna admittance for an infinitely long wire. In the time interval considered here, this quantity characterizes the admittance properties of the wire. It is observed from the curve in Figure 12 that the wire impedance dominates over the aircraft impedance except at the aircraft resonances. The aircraft resonances has the net effect of introducing an increase in the impedance as seen between the wire and the aircraft.

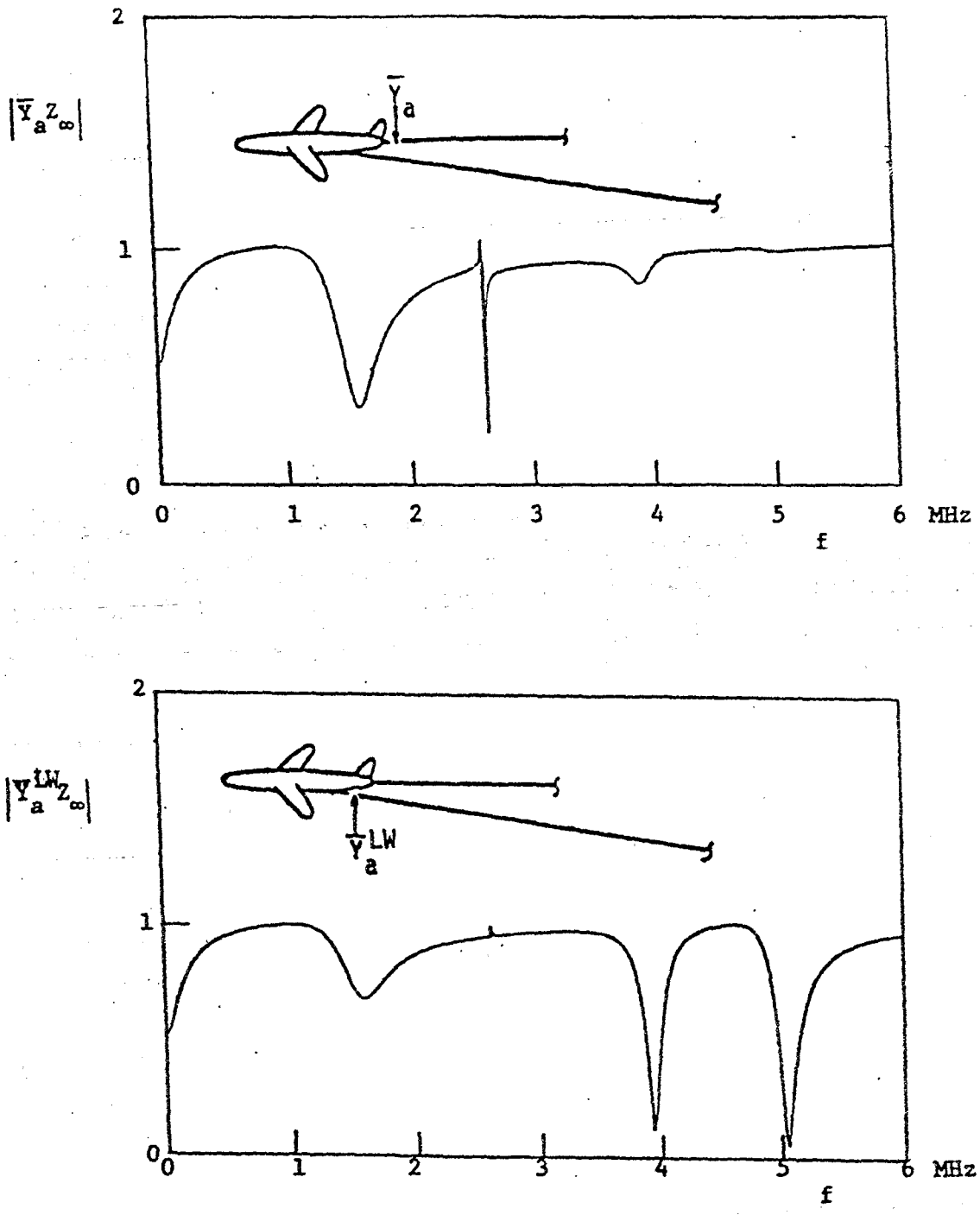

Figure 12. The admittance between the antenna wires and the aircraft.

For very low frequencies the aircraft impedance varies as $1/j\omega C_a$, $C_a (\simeq 2.5\ nF)$ being the aircraft capacitance thus resulting in the small values of $Z_\infty \bar{\bar{Y}}_a$.

Results for $\bar{\bar{Y}}_a^{LW}$ are also shown in Figure 12. The long-wire and short-wire impedances show similar properties. The differences between the curves are due to the differences in the attachment points of the two wires.

These results for the impedances show that the wires dominate $\bar{\bar{Y}}_a$ and $\bar{\bar{Y}}_a^{LW}$ over wide ranges of frequences. It is therefore resonable to expect that one can simulate the wire current using a voltage considerably below open-circuit voltage in the equivalent circuit by reducing the terminating impedance (nominally chosen to be $660\,\Omega$) in the previous section.

To understand the simulation fidelity one can expect when lowering both the output voltage and terminating impedance we study the frequency variation of the wire current under different simulation configurations. The voltage is lowered by a factor of "n" whereas the impedance is lowered by a factor of "m". Figure 13 shows how the short wire current changes with different values of m and n whereas Figure 14 shows the behavior of the long-wire current. It is observed that by keeping m and n the same one gets a smaller current the larger m and n become. This can be understood from tha fact that when Z_∞/m becomes smaller then the aircraft impedance influences the response more and more. To alleviate this problem one can choose a larger value for m than for n, i.e., reducing the impedance more than the voltage. The effects of such a scheme is also included in Figure 13 and 14. We notice that one can increase the current in certain frequency regimes (where the response is larger) whereas in other regimes not much increase is observed. The limited results here show however that it appears to be feasible to use a simulation voltage that is almost one order of magnitude less than the predicted open circuit voltage. This allows one to use a simulator voltage which is on the order of 1-2 MV for the short wire. This voltage is also sufficient for the long wire current except when the angle of incidence varies less than 30° from aft grazing incidence.

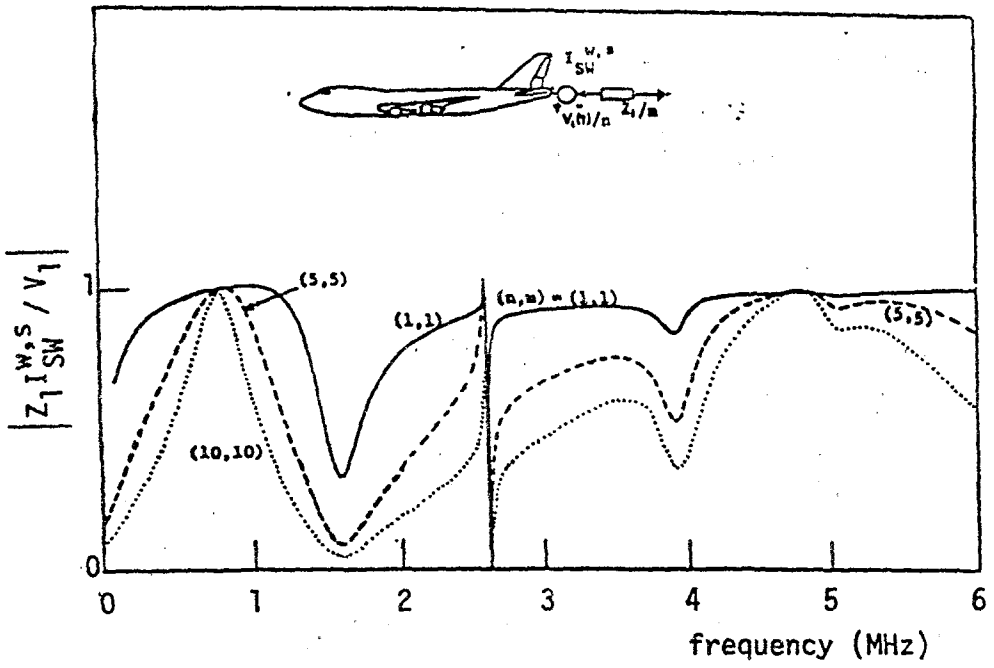

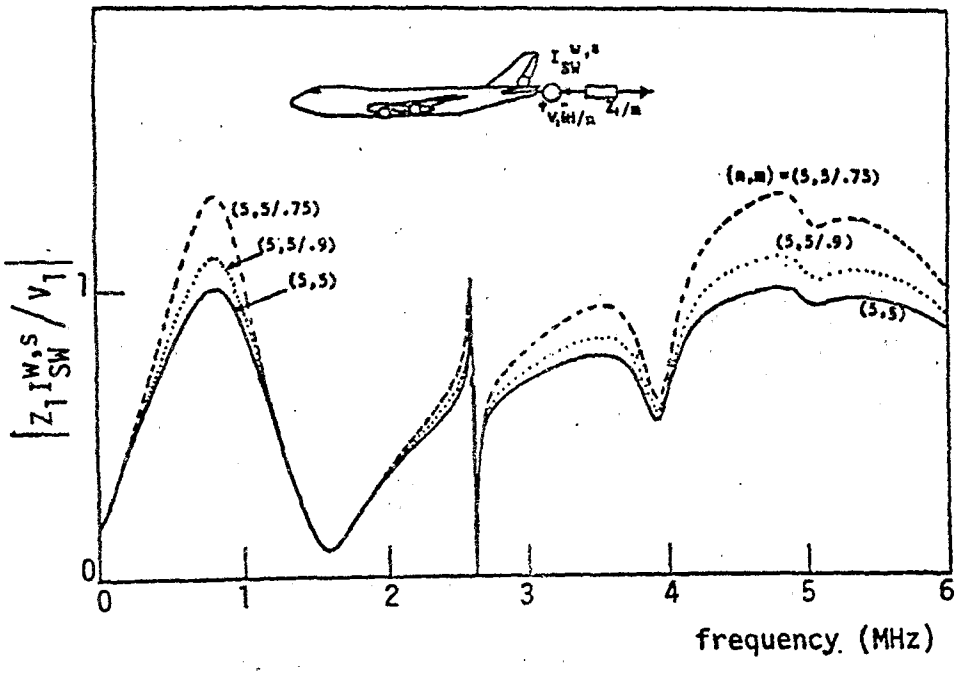

Figure 13. Normalized short wire current for different terminating impedances and exciting voltage levels.

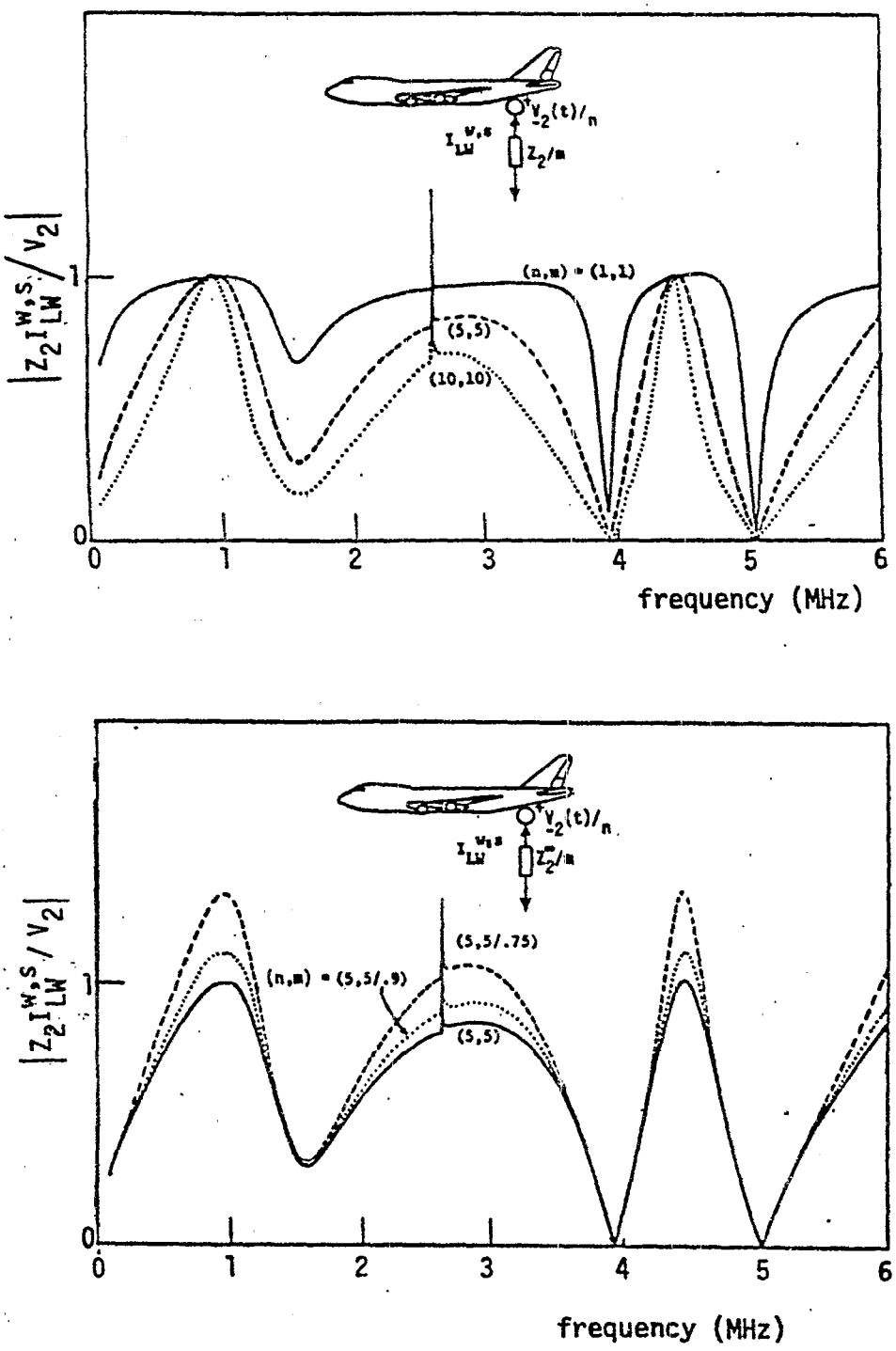

Figure 14. Normalized long-wire current for different terminating impedances and exciting voltage levels.

SECTION VI

SUMMARY AND CONCLUSIONS

The transient EMP response of the trailing-wire antenna has been analyzed. The approach used in the analysis is based on an asymptotic antenna expansion of the currents on the antenna wires and an intersecting stick model of the aircraft. The time-domain results were obtained by performing an inverse Fourier transform of the frequency-domain expressions for the induced currents. Inherently in the formulation used in this report is a linearity assumption. The effects on the trailing-wire antenna current from nonlinear corona effects are investigated separately in Reference 2.

It is found that the largest time-domain peak value of the induced current on the short wire is on the order of 20 kA whereas on the long wire current is on the order of 40 kA . The large peak values occur for angles of incidence near grazing from behind. For other angles of incidence the peak value of the short wire current is on the order of 5 kA and the long wire current 5-10 kA.

A Thévenin equivalent circuit for the antenna current is derived. It is found that the wire impedance for the early time response can be approximated by a constant value ($\simeq 660\,\Omega$). The open circuit voltage is in the 1-10 MV range for most angles of incidence. For angles close to near grazing the peak value of the open circuit voltage reaches the value of 26 MV for the long wire and 12 MV for the short wire.

Since a simulation of the early time current based directly on a synthesis of the equivalent circuit is not feasible other methods must be sought. It is observed in this report that the antenna wire impedance is much larger than the aircraft impedance for most frequencies (the main exceptions being around the aircraft resonances). By reducing the impedance in the equivalent circuit with a factor of ten or so one can reduce the open-circuit voltage with a factor of five or so and yet maintain the original current. To reduce the impedance below this value does not result in any further voltage reduction since the aircraft impedance then dominates over the simulated wire impedance. By reducing the terminating wire impedance it is possible to use a simulation voltage less than 2 MV for most angles of incidence. The maximum required voltage would be around 5 MV.

It should be mentioned that the discussion here only applies to the early-time simulation of the wire currents. Other simulation issues will be discussed in a subsequent report.

REFERENCES

1. Mini-Symposium On EMP Criteria, Simulation, Extrapolation, and Trailing Wire Response, 1980 Summer Fulmen Meeting (Fulmen 5), May 13-15 1980.

2. Charles T.C. Mo, Gregg Wilensky, "Corona Model for Trailing-Wire Antenna," RDA-TR-117900-001, November 1981.

3. F.C. Yang, V. Tatoian, L. Marin, "Frequency-Domain Response of the E-4 Trailing-Wire Antenna," Interaction Notes, Note 425, Air Force Weapons Laboratory, Kirtland AFB, NM, October 1981.

4. L. Marin, "Currents Induced on the Dual-Wire Antenna on the E-4 in the Resonance Region of the Aircraft," Dikewood Corporation, Westwood Research Branch, Los Angeles, CA 90024, Interaction Application Memos, Memo 21, June 1978.

5. L. Marin, Carl E. Baum, and J. Philip Castillo, "A Simple Way of Simulating the EMP Effects of the VLF/LF Dual-Wire Antenna on the E-4", Miscellaneous Simulator Memos, Memo 14, November 1977.

APPENDIX A

FREQUENCY - DOMAIN EXPRESSIONS FOR THE WIRE CURRENTS

In this appendix we present explicit analytical expressions for quantities used in the frequency - domain representation of the wire currents (Equations 1 and 2 of Section II).

The appropriate expressions are as follows:

$$I'_{ind} = \frac{\psi Z_o}{4\pi} \bar{Y}_T \cos k\ell_4 \times$$

$$\times \left\{ \frac{Q}{\cos k\ell_1 \cos k\ell_4} \left[I_o(\ell_1 + \ell_3 + \ell_4, \theta) + 2j \cos k\ell_1 \tan k\ell_2 \right.\right.$$

$$\left. I_o(\ell_3 + \ell_4, \theta) \right] - \frac{\Omega}{\psi} \frac{\cos\theta}{\cos k\ell_4} I_o(\ell_4, \theta) - \bar{T}_1 j \cos\theta I_o(0,\theta)$$

$$\left. + \bar{T}_2 \left[\frac{I_o(\ell_5, \pi/2-\theta)}{\cos k\ell_5} + I_o(0,\theta) - (1 + j \sin\theta \tan k\ell_5) I_o(0, \tfrac{\pi}{2} - \theta) \right] \right\} \quad (A1)$$

$$I''_{ind} = \frac{1}{\bar{T}_2 \cos k\ell_4} \left[I'_{ind} + \frac{\Omega}{\psi} \cos\theta I_o(0,\theta) \right] - \frac{\Omega}{\psi} \cos\theta I_o(\ell_4, \theta)$$

$$- \frac{\Omega}{j\psi} \frac{\tan k\ell_4}{\bar{T}_2} \left[\frac{\Omega}{\psi} \cos\theta I_o(\ell_4, \theta) - \frac{Q}{\cos k\ell_1} I_o(\ell_1 + \ell_3 + \ell_4, \theta) \right.$$

$$\left. - 2j Q \cos\theta \tan k\ell_2 I_o(\ell_3 + \ell_4, \theta) \right] \quad (A2)$$

$$\bar{Y}_a = Y_a(F(L_1) = F(L_2) = 0)$$

$$= \left\{ 1 - \frac{\Omega}{j\psi} \frac{1 + (T + j\,\Omega/\psi) \tan k\ell_4}{(1 - \tan k\ell_4 \tan k\ell_5)\,[T + j\,\Omega/\psi - \tan k(\ell_4 + \ell_5)]} \right\}^{-1} \quad (A3)$$

$$\bar{Y}_a^{LW} = Y_a^{LW} \; (F(L_1) = F(L_2) = 0)$$

$$= \bar{Y}_a \left[1 - \frac{\Omega}{j\psi} \frac{\tan k\ell_4 \; (T + \tan k\ell_5)}{(\bar{T}_1 - \bar{T}_2 \tan k\ell_5)} \right] \quad (A4)$$

$$\bar{Y}_T = Y_T(F(L_1) = F(L_2) = 0)$$

$$= \frac{\bar{Y}_a}{\cos k\ell_4} \frac{\Omega}{j\psi(\bar{T}_1 - \bar{T}_2 \tan k\ell_5)} \tag{A5}$$

$$2R_i(\theta) = 2R(\pi - \theta, L_i)$$

$$+ \frac{1+\cos\theta}{\psi} \left\{ e^{jkL_i(1+\cos\theta)} E_1\left[jkL_i(1+\cos\theta)\right] + \frac{j}{kL_i(1+\cos\theta)} \right\},$$

$$i = 1, 2 \tag{A6}$$

$$I_s(x,\theta) = \frac{\tilde{E}_o \lambda}{Z_o} \frac{j \exp(-jkx\cos\theta)}{\sin\theta \left\{ \ell n[(\Gamma ka/2)\sin\theta] + j\pi/2 \right\}} \tag{A7}$$

$$F(\xi) = \frac{\ell n \left\{ 1 - 2\pi j / \left\{ \ell n(\Gamma k^2 a^2) - \ell n[k\xi + (k^2\xi^2 + \Gamma^{-2})^{1/2}] + j\pi/2 \right\} \right\} e^{-jk\xi}}{\ell n \left\{ 1 - 2\pi j / [2\ell n(\Gamma ka) + j\pi/2] \right\}} \tag{A8}$$

$$I_o(x,\theta) = \frac{\tilde{E}_o \lambda}{Z_o} \frac{2j \exp(jkx\cos\theta)}{\Omega \sin\theta} \tag{A9}$$

$$\bar{T}_1 = T_1(F(L_2) = 0)$$

$$= T - \tan k\ell_4 + j\Omega/\psi \tag{A10}$$

$$\bar{T}_2 = T_2(F(L_2) = 0)$$

$$= (\bar{T}_1 + \tan k\ell_4 + \cot k\ell_4) \tan k\ell_4 \tag{A11}$$

$$T = Q \cos k\ell_3 (\tan k\ell_1 + 2\tan k\ell_2 + \tan k\ell_3) \tag{A12}$$

$$Q = \left[\sin k\ell_3 (\tan k\ell_1 + 2\tan k\ell_2 - \cot k\ell_3) \right]^{-1} \tag{A13}$$

$$R(\theta,\xi) = (\psi + j\pi/2)^{-1} \left[\psi - 2\ell n(\sin(\tfrac{\theta}{2})) - \exp(jv) E_1(jv) \right] \tag{A14}$$

$$v = k\xi(1 - \cos\theta) \tag{A15}$$

$$\phi = \theta - 2\theta_o, \ \Omega = 6.2 \tag{A16}$$

$$E_1(jv) = \text{the exponential integral of the first kind} \tag{A17}$$

APPENDIX. B

TIME - DOMAIN EXPRESSIONS FOR THE WIRE CURRENTS

In this appendix we present explicit analytical expressions for quantities used in the time-domain representation of the wire currents (Equations 3 to 8 of Section II).

The appropriate expressions are as follows:

$$\delta_{no} = \begin{cases} 1 \ , & n=0, \\ 0 \ , & n\neq 0, \end{cases} \tag{B1}$$

$$t_1' = L_1(1 + \cos\theta)/c, \quad t_2' = L_2(1 + \cos\phi)/c + t_2, \tag{B2}$$

$$t_2 = -\ell_4 \cos\theta/c, \tag{B3}$$

$$V_r(t) = e^{-t/\tau_r} U(t), \quad V_f(t) = e^{-t/\tau_f} U(t), \tag{B4}$$

$$V_n(t) = e^{jk_n ct} \, e^{-\beta_n ct} \, U(t) \tag{B5}$$

$$Q_n = \left. \frac{1}{\frac{d}{dk}\left[j\psi(\overline{T}_1 - \overline{T}_2 \tan k\ell_5)/\Omega - \overline{T}_2 \right]} \right|_{k = k_n} \tag{B6}$$

$$R_n = \overline{T}_2 \Big|_{k = k_n} Q_n \tag{B7}$$

$$S_n = \left[1 - \tan k\ell_4 \, (\tan k\ell_5 + \Omega/j\psi)\right]_{k = k_n} Q_n \tag{B8}$$

$$N_1(k,t) = \frac{Q \exp\left[jkc\,(t + t_{134}\cos\theta)\right]}{\sin\theta \cos k\ell_1 \cos k\ell_4} \, U\left[t - t_{134}(1 - \cos\theta)\right]$$

$$+ \frac{2j\cos\theta \tan k\ell_2 \, Q}{\sin\theta \cos k\ell_4} \, e^{jkc\,(t + t_{34}\cos\theta)} \, U\left[t - t_{34}(1 - \cos\theta)\right]$$

$$- \frac{\Omega}{\psi} \frac{\cos\theta}{\sin\theta \cos k\ell_4} e^{jkc\,(t + t_4 \cos\theta)} U\,[t - t_4(1 - \cos\theta)]$$

$$+ \frac{\bar{T}_2}{\cos\theta \cos k\ell_5} e^{jkc(t + t_5 \sin\theta)} U\,[t - t_5(1 - \sin\theta)]$$

$$+ \frac{\bar{T}_2 - j\cos\theta\,\bar{T}_1}{\sin\theta} e^{j\,kct}\, U\,(t)$$

$$- \frac{1 + j \sin\theta \tan k\ell_5}{\cos\theta} \bar{T}_2\; e^{jkct}\, U(t) \qquad \text{(B9)}$$

$$N_2(k,t) = \frac{N_1\,(k,\, t - t_4)}{\bar{T}_2 \cos k\ell_4} e^{jk\ell_4} \qquad \text{(B10)}$$

$$N_3(k,t) = \frac{\Omega}{\psi} \frac{\cos\theta}{\sin\theta} \frac{1}{\bar{T}_2 \cos k\ell_4} e^{jkct}\, U(t - t_4)$$

$$- \frac{\Omega}{\psi} \frac{\cos\theta}{\sin\theta} \left(1 + \frac{\Omega}{j\Psi} \frac{\tan k\ell_4}{\bar{T}_2}\right) e^{jkc(t + t_4 \cos\theta)} U(t + t_4 \cos\theta)$$

$$+ \frac{\Omega}{j\psi} \frac{1}{\sin\theta} \frac{Q \tan k\ell_2}{\bar{T}_2 \cos k\ell_1} e^{jkc(t + t_{134} \cos\theta)} U\,[t - t_{134}(1 - \cos\theta) + t_4]$$

$$+ \frac{2\Omega}{\psi} \frac{\tan k\ell_2 \tan k\ell_4 \cos\theta\, Q}{\bar{T}_2 \sin\theta} e^{jkc(t + t_{34} \cos\theta)} U\left[t - t_{34}(1 - \cos\theta) + t_4\right] \qquad \text{(B11)}$$

$$t_{134} = (\ell_1 + \ell_3 + \ell_4)/c, \quad t_{34} = (\ell_3 + \ell_4)/c, \qquad \text{(B12)}$$

$$t_4 = \ell_4/c, \quad t_5 = \ell_5/c \qquad \text{(B13)}$$

and a_θ, a_ϕ are slowly varying functions of θ, ϕ, respectively, and can be approximated by $a_\theta \simeq a_\phi \simeq 2$.